Reactive and Functional Polymers xxx (2016) xxx–xxx

Contents lists available at ScienceDirect

Reactive and Functional Polymers

journal homepage: www.elsevier.com/locate/react

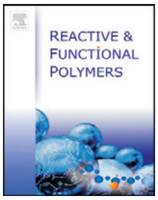

Triphenylamine-based redox-active aramids with 1-piperidinyl substituent as an auxiliary donor: Enhanced electrochemical stability and electrochromic performance

Sheng-Huei Hsiao [a,*], Ying-Hsiu Hsiao [b], Yu-Ruei Kung [c], Chyi-Ming Leu [c], Tzong-Ming Lee [c]

[a] *Department of Chemical Engineering and Biotechnology, National Taipei University of Technology, Taipei 10608, Taiwan*
[b] *Department of Chemical Engineering, Tatung University, Taipei 10451, Taiwan*
[c] *Department of Opto-Electronic Nano Hybrid Materials Research, Material and Chemical Research Laboratories, Industrial Technology Research Institute, Hsinchu 31040, Taiwan*

ARTICLE INFO

Article history:
Received 16 January 2016
Received in revised form 24 March 2016
Accepted 25 March 2016
Available online xxxx

Keywords:
Piperidine
Triphenylamine
Redox Polyamides
Electrochemistry
Electrochromism

ABSTRACT

A new triphenylamine-based diamine monomer 4,4′-diamino-4″-(1-piperidinyl)triphenylamine was synthesized and polymerized with various aromatic dicarboxylic acids via the phosphorylation polyamidation technique leading to a series of redox-active aromatic polyamides (aramids). All the aramids exhibit good solubility in many organic solvents and can be solution-cast into flexible and strong films with high thermal stability. Cyclic voltammograms of the polymer films on the indium-tin oxide (ITO)-coated glass substrate exhibit a pair of well-defined and reversible oxidation waves with very low onset potentials of 0.27–0.35 V (vs. Ag/AgCl) in acetonitrile solution, with a strong color change from colorless neutral form to green and deep blue oxidized forms in the range of 0.75–1.20 V. The optical transmittance change (Δ%T) at 636 nm between the neutral state and the fully oxidized state is up to 83%.

1. Introduction

Electrochromism is well-known as the reversible color change of an electroactive species upon electrochemical oxidation or reduction [1,2]. This unique property is of great interest for a wide range of applications, such as smart windows [3,4], color changing eyewear [5,6], display devices [7,8], and military camouflage [9]. Recent high-profile commercialization of electrochromic materials includes the Boeing 787 Dreamliner windows manufactured by Gentex [10]. Metal oxides [11,12], organic π-conjugated polymers [13–16], and metallo-supramolecular coordination polymers [17–20] are frequently used for electrochromic studies. In particular, π-conjugated polymers have attracted tremendous attention because of combined several advantages such as mechanical flexibility, high optical contrast ratios, long-term redox stability and easy color tuning through structural control [21–25].

Aromatic polyamides (aramids) are well accepted as high-performance polymers because of their good thermal and chemical stability, excellent mechanical properties, and high glass transition temperatures [26]. However, these polymers are difficult to process due to their high glass transition temperatures (T_g), or high melting temperatures (T_m), and limited solubility in organic solvents. Considerable efforts have been made to improve the solubility and melting processability of polymers while maintaining their positive properties [27]. A variety of structural modifications to the polymer backbone, such as insertion of flexible linkage on main chain, utilization of noncoplanar or asymmetric monomers, and incorporation of pendent groups in the polymer backbone, can be used to modify the polymer properties, either by lowering the inter-chain interaction or by reducing the stiffness of the polymer chain [28–42]. Depending on the type and amount of structural modification, the melting temperatures can be lowered and the solubility improved, resulting in processable aramids. It has also been demonstrated that incorporating the rigid three-dimensional structure of triphenylamine (TPA) into the aramid backbones reduces the polymer chain packing and improves the solubility [43–45].

On the other hand, TPA derivatives and polymers are well-known for their electroactive and photoactive properties that may find optoelectronic applications as photoconductors, hole-transporters, and light-emitters [46,47]. TPAs can be easily oxidized to form stable radical cations as long as the para-position of the phenyl rings is protected [48–50]. Since 2005, we have performed extensive studies on the design and synthesis of high-performance polymers (typically aromatic polyimides and polyamides) bearing TPA unit as redox-chromophore for potential electrochromic applications [51,52]. It has also been demonstrated that incorporation of electron-donating substituent at the para position of TPA can afford a stable radical cation thus enhancing the electrochemical and electrochromic stability of the polymers [53–55]. As a continuation of our efforts in developing electrochromic materials with long-term stability, rapid redox switching, and high optical contrast between their bleached and colored states, herein we

---

[*] Corresponding author.

http://dx.doi.org/10.1016/j.reactfunctpolym.2016.03.020

synthesize a new diamine monomer, 4,4′-diamino-4″-(1-piperidinyl)triphenylamine, and its derived aramids containing the electroactive TPA unit with 1-piperidinyl substituent as an auxiliary donor. We anticipated that incorporating (1-piperidinyl)TPA unit into the aramid backbone could improve the solubility, electrochemical stability, and electrochromic performance.

2. Experimental section

2.1. Materials

Piperidine (Tedia), 4-fluoronitrobenzene (Acros), potassium carbonate (K_2CO_3) (Showa), cesium fluoride (CsF) (Acros), dimethyl sulfoxide (DMSO), 10% palladium on charcoal (Pd/C) (Fluka), hydrazine monohydrate (TCI) were used as received. *N*,*N*-Dimethylacetamide (DMAc) (Tedia), *N*,*N*-dimethylformamide (DMF) (Tedia), triphenyl phosphite (TPP) (Acros), pyridine (Py) (Wako) and *N*-methyl-2-pyrrolidone (NMP) (Tedia) were dried over calcium hydride for 24 h, distilled under reduced pressure, and stored over 4 Å molecular sieves in a sealed bottle. The commercially available aromatic dicarboxylic acids including terephthalic acid (**5a**) (Wako), isophthalic acid (**5b**) (Wako), 4,4′-biphenydicarboxylic acid (**5c**) (TCI), 4,4′-dicarboxydiphenyl ether (**5d**) (TCI), bis(4-carboxyphenyl) sulfone (**5e**) (New Japan Chemicals Co.), 2,2-bis(4-carboxyphenyl)hexafluoropropane (**5f**) (TCI), 1,4-naphthalenedicarboxylic acid (**5g**) (Wako), and 2,6-naphthalenedicarboxylic acid (**5h**) (TCI) were used as received. Commercially obtained calcium chloride ($CaCl_2$) (Wako) was dried under vacuum at 180 °C for 8 h prior to use. Tetrabutylammonium perchlorate (TBAP) (Acros) was dried in vacuo before use. All other reagents were used as received from commercial sources.

2.2. Synthesis of (1-piperidinyl)TPA diamine monomer

2.2.1. 1-(4-Nitrophenyl)piperidine (**1**)

In a 250 mL round-bottom flask equipped with a stirring bar, a mixture of 12.8 g (0.15 mol) of piperidine, 21.2 g (0.15 mol) of 4-fluoronitrobenzene, and 20.7 g (0.15 mol) of potassium carbonate (K_2CO_3) in 100 mL of dimethyl sulfoxide (DMSO) was heated with stirring at 120 °C for 20 h. After cooling, the mixture was poured into 400 mL mixed solution of ethanol/water (1:1). The yellow crystals were collected by filtration with a yield of 30.0 g (97%) and a melting point of 100–102 °C, measured by differential scanning calorimetry (DSC) at a scan rate of 10 °C/min. IR (KBr):1577, 1329 cm^{-1} (—NO_2 str.). ^1H NMR (500 MHz, DMSO-d_6, δ, ppm): 8.02 (d, $J = 9.5$ Hz, 2H, H_e), 6.98 (d, $J = 9.5$ Hz, 2H, H_d), 3.49 (t, $J = 5.7$ Hz, 4H, H_c), 1.63 (m, 2H, H_a), 1.57 (m, 4H, H_b). ^{13}C NMR (125 MHz, DMSO-d_6, δ, ppm): 154.5 (C^4), 135.9 (C^7), 125.8 (C^6) 112.2 (C^5), 47.5 (C^3), 24.8 (C^2), 23.8 (C^1).

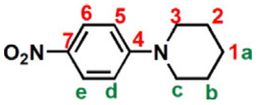

2.2.2. 4-(1-Piperidinyl)aniline (**2**)

In a 500 mL round-bottom flask, 28.3 g (0.14 mol) of nitro compound **1**, 0.2 g of 10 wt% Pd/C, 20 mL hydrazine monohydrate and 180 mL of ethanol was stirred at a reflux temperature for 10 h. The solution was filtered hot to remove Pd/C, and the filtrate was evaporated under reduced pressure to dryness. A deep purplish red liquid was obtained. The product (**2**) was used for the next step without further purification. The yield was 18.1 g (75%). IR (KBr): 3429, 3346 cm^{-1} (—NH_2 str.). ^1H NMR (500 MHz, DMSO-d_6, δ, ppm): 6.66 (d, $J = 8.8$ Hz, 2H, H_e), 6.48 (d, $J = 8.8$ Hz, 2H, H_d), 4.49 (s, 2H, —NH_2), 2.84 (t, $J = 5.4$ Hz, 4H, H_c), 1.59 (m, 4H, H_b), 1.45 (m, 2H, H_a). ^{13}C NMR (125 MHz, DMSO-d_6, δ, ppm): 143.5 (C^4), 141.9 (C^7), 118.6 (C^6), 114.7 (C^5), 52.1 (C^3), 25.8 (C^2), 23.8 (C^1).

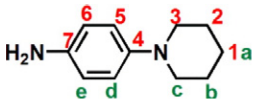

2.2.3. 4,4′-Dinitro-4″-(1-piperidinyl)triphenylamine (**3**)

In a 250 mL round-bottom flask equipped with a stirring bar, a mixture of 12.0 g (0.068 mol) of amino compound **2**, 19.2 g (0.136 mol) of 4-fluoronitrobenzene, and 20.7 g (0.136 mol) of cesium fluoride (CsF) in 100 mL of dimethyl sulfoxide (DMSO) was heated with stirring at 120 °C for 20 h. After cooling, the mixture was poured into 400 mL mixed solution of ethanol/water (1:1), and the dark red precipitate was collected by filtration. Recrystallization from DMF/H_2O yielded 18.5 g of the desired dinitro compound (**3**) as red crystals in 65% yield. [mp: 168–171 °C, measured by differential scanning calorimetry (DSC) at a scan rate of 10 °C/min]. IR (KBr): 1579, 1340 cm^{-1} (—NO_2 str.). ^1H NMR (500 MHz, DMSO-d_6, δ, ppm): 8.15 (d, $J = 9.2$ Hz, 4H, H_g), 7.17 (d, $J = 9.2$ Hz, 4H, H_f), 7.07 (d, $J = 9.0$ Hz, 2H, H_e), 7.02 (d, $J = 9.0$ Hz, 2H, H_d), 3.20 (t, $J = 5.6$ Hz, 4H, H_c), 1.62 (m, 4H, H_b), 1.55 (m, 2H, H_a). ^{13}C NMR (125 MHz, DMSO-d_6, δ, ppm): 151.7 (C^8), 150.3 (C^4), 141.5 (C^{11}), 134.1 (C^7), 128.4 (C^6), 125.4 (C^{10}), 121.6 (C^9), 116.7 (C^5), 48.8 (C^3), 25.1 (C^2), 23.7 (C^1).

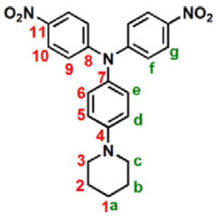

2.2.4. 4,4′-Diamino-4″-(1-piperidinyl)triphenylamine (**4**)

In a 500 mL round-bottom flask, 10 g (0.024 mol) of dinitro compound **3**, 0.15 g of 10 wt% Pd/C, 8 mL hydrazine monohydrate and 100 mL of ethanol was stirred at a reflux temperature for 12 h. The solution was filtered hot to remove Pd/C, and the filtrate was then cooled to precipitate white needles. The product (**4**) was collected by filtration and dried in vacuo at 70 °C to give 5.5 g (yield 73%) of diamine **4** as white needles. [mp: 172–174 °C, measured by differential scanning calorimetry (DSC) at a scan rate of 10 °C/min]. IR (KBr): 3338, 3291 cm^{-1} (—NH_2 str.). ANAL. Calculated for $C_{23}H_{26}N_4$ (358.48): C, 77.06%; H, 7.31%; N, 15.63%. Found: C, 76.86%; H, 7.26%; N, 15.63%. ^1H NMR (500 MHz, DMSO-d_6, δ, ppm): 6.74 (d, $J = 9.1$ Hz, 2H, H_d), 6.68 (d, $J = 8.6$ Hz, 4H, H_f), 6.65 (d, $J = 9.0$ Hz, 2H, H_e), 6.49 (d, $J = 8.7$ Hz, 4H, H_g), 4.79 (s, 4H, —NH_2), 2.95 (t, $J = 5.4$ Hz, 4H, H_c), 1.59 (m, 4H, H_b), 1.47 (m, 2H, H_a). ^{13}C NMR (125 MHz, DMSO-d_6, δ, ppm): 145.5 (C^{11}), 144.02 (C^8), 141.8 (C^4), 137.5 (C^7), 125.4 (C^9), 120.8 (C^6), 117.3 (C^5), 114.7 (C^{10}), 50.7 (C^3), 25.5 (C^2), 23.7 (C^1).

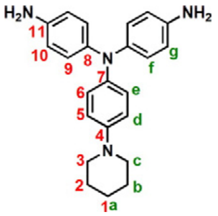

Please cite this article as: S.-H. Hsiao, et al., Triphenylamine-based redox-active aramids with 1-piperidinyl substituent as an auxiliary donor: Enhanced electrochemical stability..., Reactive and Functional Polymers (2016), http://dx.doi.org/10.1016/j.reactfunctpolym.2016.03.020

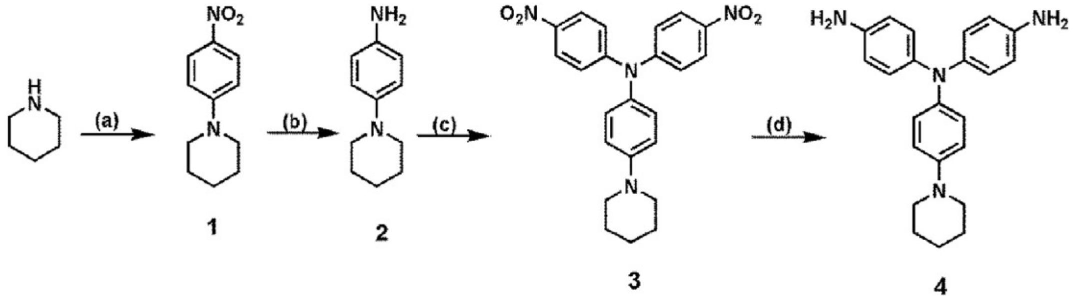

Scheme 1. Synthetic route to the target diamine monomer **4**: (a) *p*-fluoronitrobenzene, K_2CO_3, DMSO, 120 °C, 20 h; (b) hydrazine, Pd/C, EtOH, reflux, 10 h; (c) *p*-fluoronitrobenzene, CsF, DMSO, 120 °C, 20 h; (d) hydrazine, Pd/C, EtOH, reflux, 12 h.

2.3. Synthesis of polyamides

The synthesis of polyamide **6a** is used as an example to illustrate the general synthetic route used to produce the **6** series polyamides. A 50 mL round-bottom flask equipped with a magnetic stirrer was charged with 0.5377 g (1.50 mmol) of diamine monomer **4**, 0.2492 g (1.50 mmol) of terephthalic acid (**5a**), 1.5 mL of TPP, 2 mL of NMP, 0.5 mL of pyridine, and 0.2 g of calcium chloride ($CaCl_2$). The reaction mixture was heated with stirring at 110 °C for 3 h. The resulting polymer solution was poured slowly into 200 mL of stirring methanol giving rise to a stringy, fiber-like precipitate that was collected by filtration, washed thoroughly with hot water and methanol, and dried. IR (film): 3282 (amide N—H stretch), 1653 cm^{-1} (amide C=O stretch). The other polyamides were prepared by an analogous procedure.

2.4. Measurements

Infrared (IR) spectra were recorded on a Horiba FT-720 FT-IR spectrometer. Elemental analyses were run in a Heraeus Vario EL III CHNS elemental analyzer. ^1H and ^{13}C NMR spectra were measured on a Bruker AVANCE 500 FT-NMR system with tetramethylsilane as an internal standard. The inherent viscosities were determined with a Cannon-Fenske viscometer at 30 °C. Wide-angle X-ray diffraction (WAXD) measurements were performed at room temperature (ca. 25 °C) on a Shimadzu XRD-6000 X-ray diffractometer with a graphite monochromator (operating at 40 kV and 30 mA), using nickel-filtered Cu-Kα radiation ($\lambda = 1.5418$ Å). The scanning rate was 2°/min over a range of $2\theta = 10$–40°. Thermogravimetric analysis (TGA) was performed with a Perkin-Elmer Pyris 1 TGA. Experiments were carried out on approximately 4–6 mg of samples heated in flowing nitrogen or air (flow rate = 40 cm^3/min) at a heating rate of 20 °C/min. DSC analyses were performed on a Perkin-Elmer Pyris 1 DSC at a scan rate of 20 °C/min in flowing nitrogen. Thermomechanical analysis (TMA) was determined with a Perkin-Elmer TMA 7 instrument. The TMA experiments were carried out from 50 to 350 °C at a scan rate of 10 °C/min with a penetration probe 1.0 mm in diameter under an applied constant load of 10 mN. Softening temperatures (T_s) were taken as the onset temperatures of probe displacement on the TMA traces. Electrochemistry was performed with a CH Instruments 600c electrochemical analyzer. Voltammograms are presented with the positive potential pointing to the left and with increasing anodic currents pointing downwards. Cyclic

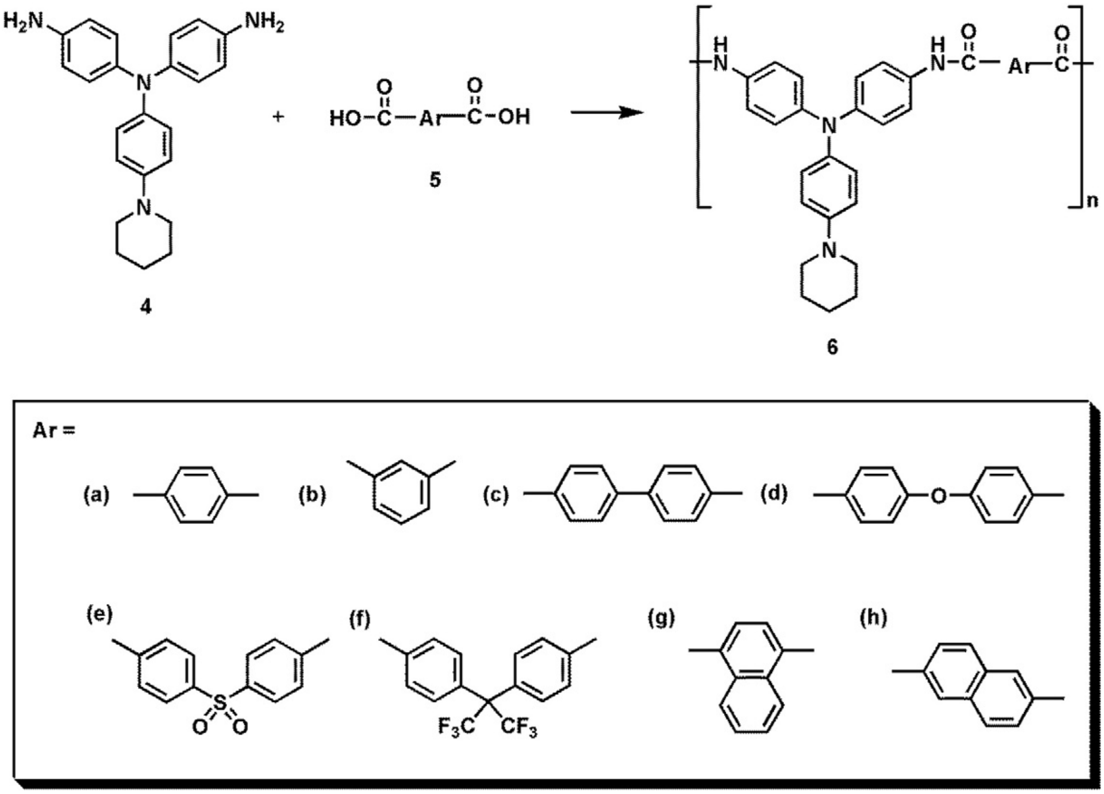

Scheme 2. Synthesis of polyamides **6a–6h**.

Please cite this article as: S.-H. Hsiao, et al., Triphenylamine-based redox-active aramids with 1-piperidinyl substituent as an auxiliary donor: Enhanced electrochemical stability..., Reactive and Functional Polymers (2016), http://dx.doi.org/10.1016/j.reactfunctpolym.2016.03.020

Table 1
Inherent viscosity and solubility behavior of polyamides.[a, b]

Polymer code	η_{inh}[a] (dL/g)	Solubility in various solvents[b]					
		NMP	DMAc	DMF	DMSO	*m*-Cresol	THF
6a	0.63	+	+	+h	+	+h	−
6b	0.42	+h	+h	+h	+h	±	−
6c	0.90	+h	+h	+h	+	+h	−
6d	0.72	+	+	+h	+	+h	−
6e	0.55	+	+	+	+	+h	−
6f	0.60	+	+	+	+	+h	−
6g	0.61	+	+	+	+	+h	−
6h	0.86	+h	+h	+h	+h	±	−

Solubility: +: soluble at room temperature; ±: partially soluble; +h: soluble on heating; −: insoluble even on heating.
Solvents: NMP: *N*-methyl-2-pyrrolidone; DMAc: *N*,*N*-dimethylacetamide; DMF: *N*,*N*-dimethylformamide; DMSO: dimethyl sulfoxide; THF: tetrahydrofuran.

[a] Inherent viscosity measured at a concentration of 0.5 dL/g in DMAc — 5 wt% LiCl at 30 °C.

[b] The solubility was determined with a 10 mg sample in 1 mL of a solvent.

Table 2
Thermal properties of polyamides[a].

Polymer code	T_g[b] (°C)	T_s[c] (°C)	T_d at 5 wt% loss[d] (°C)		T_d at 10 wt% loss[d] (°C)		Char yield (%)[e]
			In N_2	In air	In N_2	In air	
6a	287 (295)[f]	283	400	411	437	434	66
6b	281 (290)	278	435	432	476	478	72
6c	289 (302)	285	450	428	511	489	73
6d	274 (283)	273	439	448	486	511	69
6e	290 (296)	282	411	412	437	433	63
6f	284 (288)	283	474	465	535	512	63
6g	290 (295)	288	419	420	456	450	63
6h	297 (307)	295	422	435	455	489	71

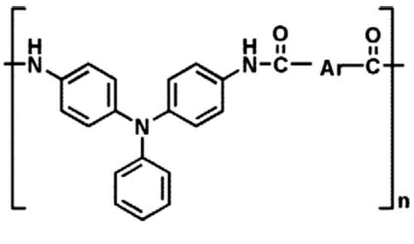

6'

[a] The polymer film samples were heated at 300 °C for 30 min prior to all the thermal analyses.

[b] The samples were heated from 50 to 400 °C at a scan rate of 20 °C/min followed by rapid cooling to 50 °C at −200 °C/min in nitrogen. The midpoint temperature of baseline shift on the subsequent DSC trace (from 50 to 400 °C at heating rate 20 °C/min) was defined as T_g.

[c] Softening temperature measured by TMA using a penetration method.

[d] Decomposition temperature at which a 5% or 10% weight loss was recorded by TGA at a heating rate of 20 °C/min.

[e] Residual weight percentages at 800 °C under nitrogen flow.

[f] Values in parentheses are data of analogous polyamides **6′** having the corresponding diacid residue as in the **6** series.

voltammetry was conducted with the use of a three-electrode cell in which ITO (polymer films area about 0.8 cm × 1.25 cm) was used as a working electrode. A platinum wire was used as an auxiliary electrode. All cell potentials were taken with the use of a home-made Ag/AgCl, KCl (sat.) reference electrode. Ferrocene was used as an external reference for calibration (+0.44 V vs. Ag/AgCl). Spectroelectrochemical and electrochromic properties of the polymer films on ITO-glass were studied by a CH Instruments 600c electrochemical analyzer along with an Agilent 8453 UV–Visible photodiode array spectrophotometer.

3. Results and discussion

3.1. Monomer synthesis

The new triphenylamine-based diamine monomer having a pendent piperidinyl group, namely 4,4′-diamino-4″-(1-piperidinyl)triphenylamine (**4**), was prepared by a four-step reaction sequence outlined in Scheme 1. 4-(1-Piperidinyl)aniline (**2**) was prepared by the condensation of piperidine with 4-fluoronitrobenzene followed by hydrazine Pd/C-catalytic reduction of the intermediate compound 1-(4-nitrophenyl)piperidine (**1**). The target diamine monomer **4** was successfully synthesized by the double *N*-arylation reactions of compound **2** with 4-fluoronitrobenzene and the subsequent catalytic reduction of the intermediate compound 4,4′-dinitro-4″-(1-piperidinyl)triphenylamine (**3**) by means of hydrazine and Pd/C catalyst. FT-IR, ^{1}H NMR and ^{13}C NMR spectroscopic techniques were used to identify the structures of all the synthesized compounds **1**–**4**. Fig. S1 (Supporting Information) shows the FT-IR spectra of the synthesized compounds **1** to **4**. The nitro groups of compounds **1** and **3** gave two characteristic bands at around 1580 and 1330–1340 cm^{-1} (—NO_2 asymmetric and symmetric stretching). After reduction, the

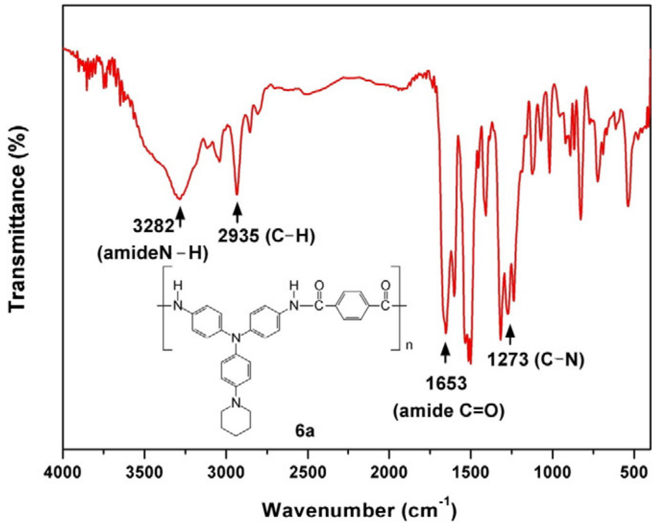

Fig. 1. Typical IR spectrum of polyamide **6a**.

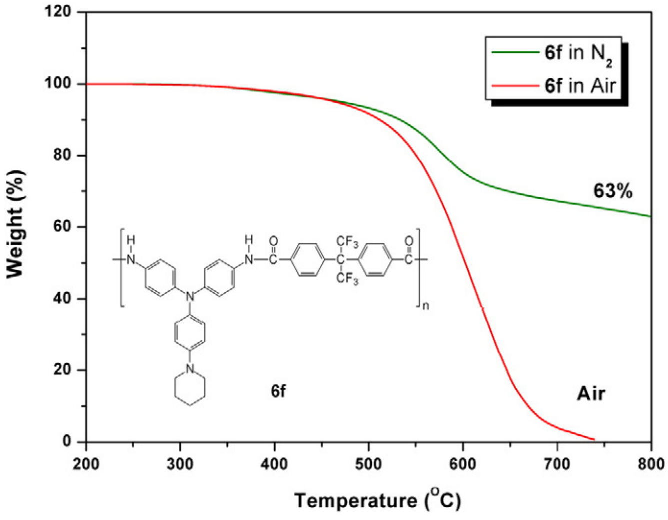

Fig. 2. TGA thermograms of polyamide **6f** with heating rate 20 °C/min.

Please cite this article as: S.-H. Hsiao, et al., Triphenylamine-based redox-active aramids with 1-piperidinyl substituent as an auxiliary donor: Enhanced electrochemical stability..., Reactive and Functional Polymers (2016), http://dx.doi.org/10.1016/j.reactfunctpolym.2016.03.020

characteristic absorptions of the nitro group disappeared and the primary amino group showed the typical N—H stretching absorptions in the region of 3200–3500 cm^{-1}. The ^{1}H and ^{13}C NMR spectra of compounds **1** to **4** are illustrated in Figs. S2 and S3, respectively. Assignments of each hydrogen and carbon are assisted by the two-dimensional NMR spectra. The H—H COSY and C—H COSY spectra of compound **4** are shown in Figs. S4 and S5, respectively, and these spectra agree well with the proposed molecular structure of the targeted diamine monomer.

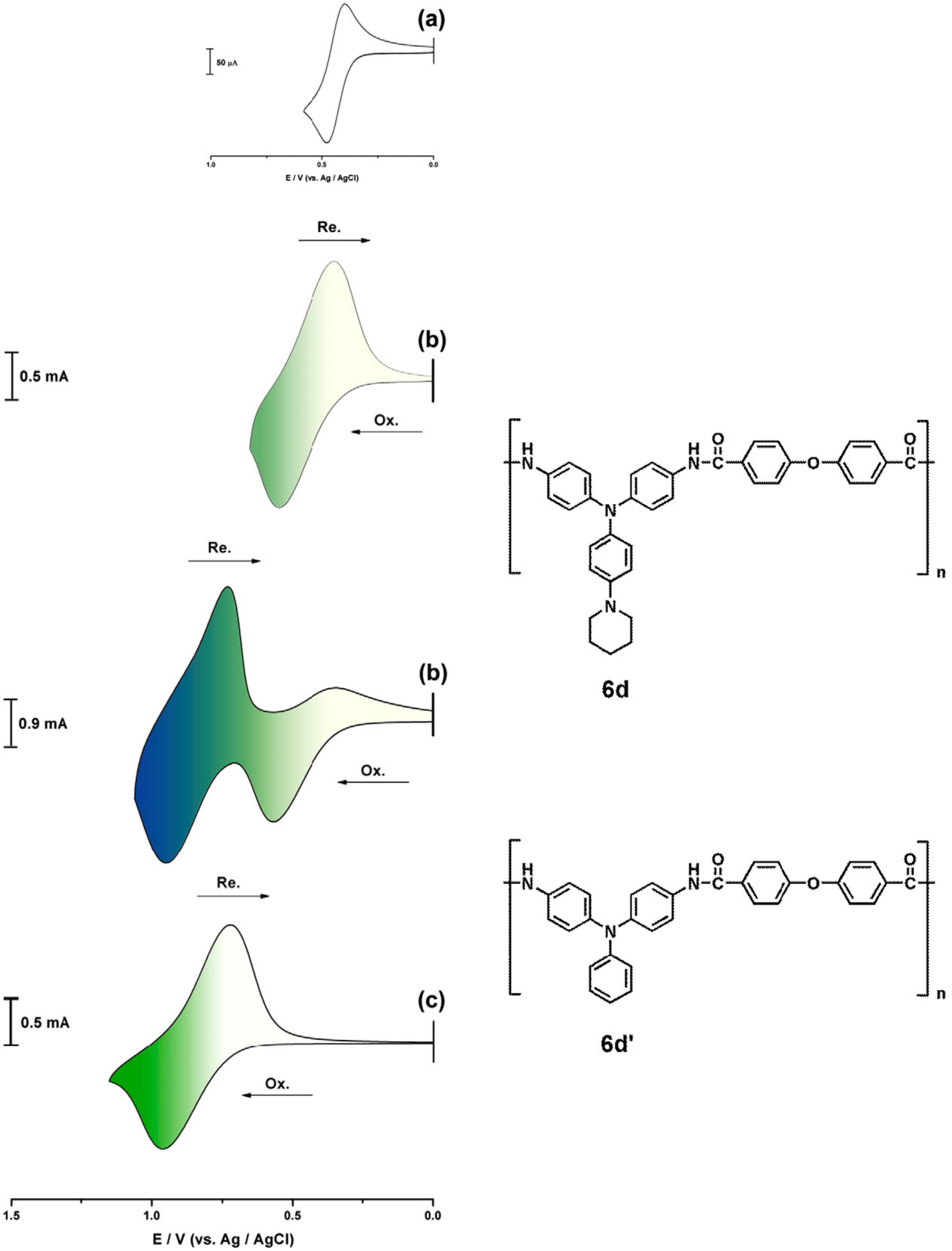

Fig. 3. CV diagrams of (a) ferrocene and the films of polyamides (b) **6d** and (c) **6d′** on an ITO-coated glass substrate in MeCN containing 0.1 M TBAP at a scan rate of 100 mV/s. Polyamide **6d** was measured in two different potential ranges: 0–0.7 and 0–1.2 V.

Please cite this article as: S.-H. Hsiao, et al., Triphenylamine-based redox-active aramids with 1-piperidinyl substituent as an auxiliary donor: Enhanced electrochemical stability..., Reactive and Functional Polymers (2016), http://dx.doi.org/10.1016/j.reactfunctpolym.2016.03.020

3.2. Polymer synthesis

According to the phosphorylation technique described by Yamazaki and co-workers [56], a series of novel TPA-based aramids, **6a**–**6h**, with 1-piperidinyl para-substituted on the pendent phenyl ring were prepared from the diamine **4** and various aromatic dicarboxylic diacids (**5a**–**5h**) by the direct polycondensation reaction with triphenyl phosphate (TPP) and pyridine as condensing agents (Scheme 2). All the polymerizations proceeded homogeneously throughout the reaction and afforded clear, highly viscous polymer solutions. These polymers precipitated in a tough, fiber-like form when the resulting polymer solutions were slowly poured with stirring into methanol. These polyamides were obtained in almost quantitative yields, with η_{inh} values in the range of 0.42–0.90 dL/g, as summarized in Table 1. Structural features of these aramids were verified by FTIR spectra based on characteristic absorption bands observed around 3280 (amide N—H stretching), 1650 (carbonyl C═O stretching), 1270 (amine C—N stretching). Fig. 1 illustrates a typical FTIR spectrum of the representative polyamide **6a**. All the polymers can be solution-cast into flexible and tough films (see Fig. S6), and this is indicative of the formation of high molecular weight polymers. For a comparative purpose, referenced polyamides **6a′**–**6h′** were prepared from dicarboxylic acids **5a**–**5h** and 4,4′-diaminotriphenylamine in a similar synthetic procedure used for the **6** series polyamides.

3.3. Properties of polymers

3.3.1. Solubility and film property

The solubility properties of polyamides **6a**–**6h** in several organic solvents at 10% (*w*/*v*) are summarized in Table 1. All the polyamides could be dissolved in polar solvents such as NMP, DMAc, DMF, and DMSO at room temperature or upon heating at 100 °C. This can be attributed in part to the incorporation of bulky, three-dimensional 4-piperidinotriphenylamine groups, which retard dense chain packing and lead to a decreased interchain interaction. Therefore, the good solubility makes these polymers potential candidates for solution processing. All of the polymers could afford flexible and tough films, and they were amorphous in nature as evidenced by wide-angle X-ray diffraction (WAXD) patterns (Fig. S7).

3.3.2. Thermal properties

The thermal properties of polyamides were examined by DSC, TMA and TGA. The thermal behavior data of all the polymers are summarized in Table 2. The glass-transition temperatures (T_g) of the polyamides **6a**–**6h** were observed in the range of 274–297 °C by DSC. The lower T_g value of **6d** can be explained in terms of the flexibility and low rotation barrier of its diacid moiety. In most cases, the **6** series polyamides showed slightly lower T_g values than those of the corresponding **6′** analogs

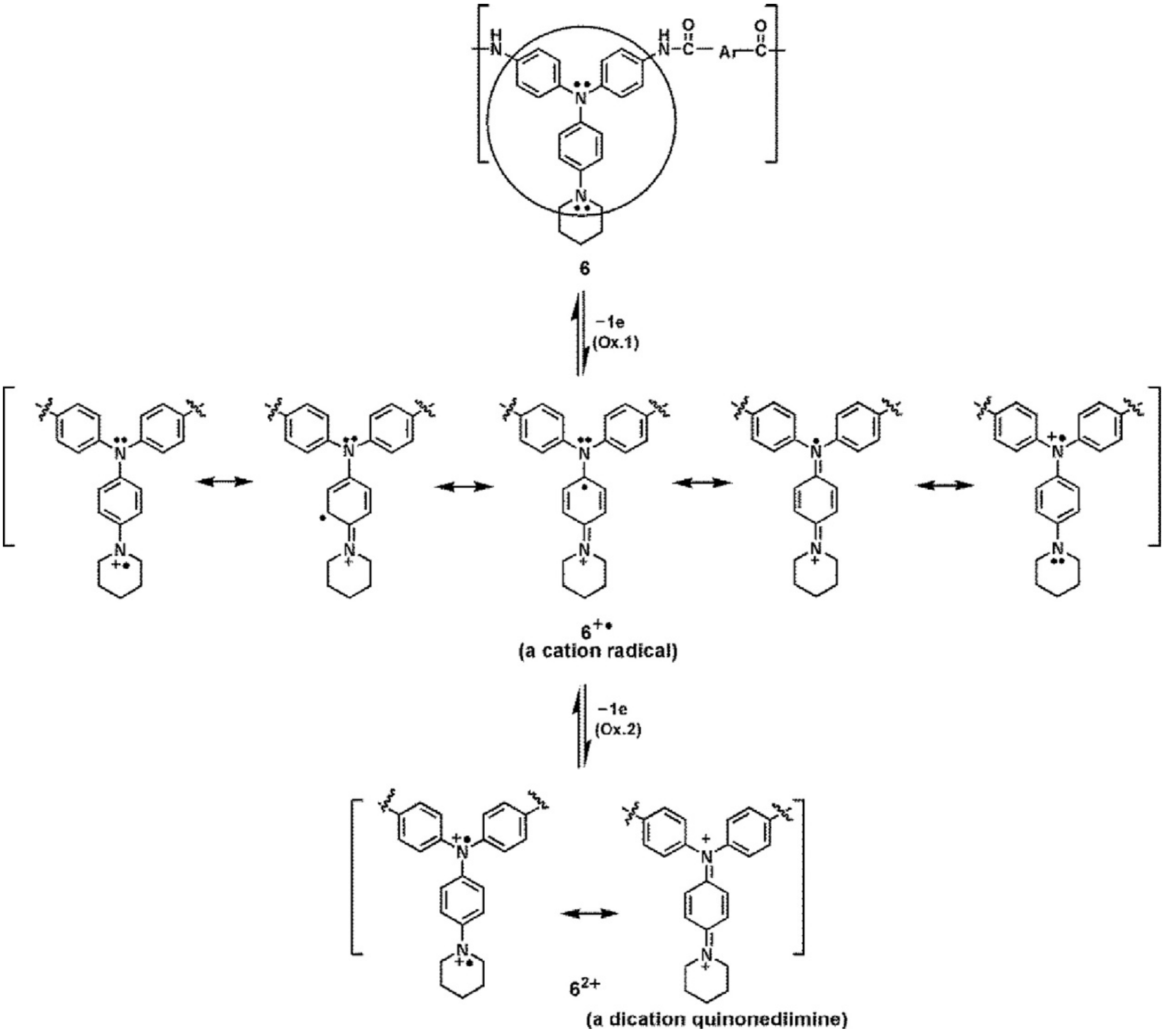

Scheme 3. Proposed oxidation pathways of the (1-piperidinyl)TPA segment in the **6** series polyamides.

Please cite this article as: S.-H. Hsiao, et al., Triphenylamine-based redox-active aramids with 1-piperidinyl substituent as an auxiliary donor: Enhanced electrochemical stability..., Reactive and Functional Polymers (2016), http://dx.doi.org/10.1016/j.reactfunctpolym.2016.03.020

Table 3
Electrochemical properties of the polyamides.

Code	E_{onset} (V)[a]	$E_{1/2}$ (V)[b] (vs. Ag/AgCl)		E_g (eV)[c]	HOMO (eV)[d]		LUMO (eV)[e]	
		Ox. 1	Ox. 2		E_{onset}	$E_{1/2}$	E_{onset}	$E_{1/2}$
6a	0.27	0.44 (0.87)[f]	0.82	2.70	4.70	4.80	2.00	2.10
6b	0.32	0.47 (0.85)	0.84	2.86	4.75	4.83	1.89	1.97
6c	0.29	0.47 (0.86)	0.86	2.76	4.72	4.83	1.96	2.07
6d	0.35	0.46 (0.86)	0.84	2.93	4.78	4.82	1.85	1.89
6e	0.30	0.48 (0.88)	0.85	2.62	4.73	4.84	2.11	2.22
6f	0.33	0.46 (0.88)	0.83	2.79	4.76	4.82	1.97	2.03
6g	0.34	0.49 (0.85)	0.84	2.92	4.77	4.85	1.85	1.93
6h	0.28	0.47 (0.85)	0.88	3.00	4.71	4.83	1.71	1.83

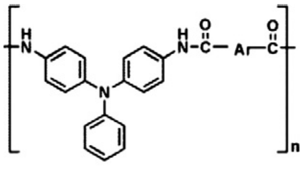

6'

[a] Onset oxidation potentials from cyclic voltammograms.

[b] Oxidation half-wave potentials from cyclic voltammograms.

[c] Energy band gap calculated from absorption edge of the polymer film according to the following equation: $E_g = 1240/\lambda_{abs,onset}$.

[d] The HOMO energy levels were calculated from E_{onset} or $E_{1/2}$ values and were referenced to ferrocene (4.8 eV).

[e] LUMO = HOMO − E_g.

[f] Values in parentheses are data of the parent polyamides **6′** having the corresponding diacid residue as in the **6** series.

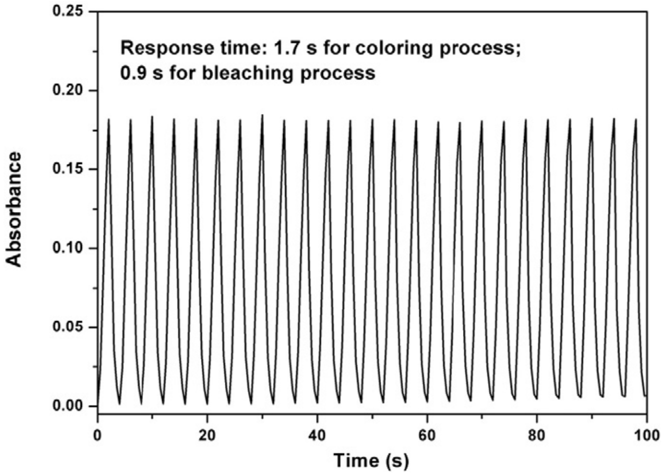

Fig. 5. Optical switching for polyamide **6d** at λ_{max} = 805 nm as the applied voltage was stepped between 0 and 0.75 V (vs. Ag/AgCl).

without the piperidinyl substituent. This result might be attributed to the internal plasticization effect of the piperidinyl substituent in the **6** series polyamides. The softening temperatures (T_s) of the polymer films were determined with TMA by the penetration method. The T_s value was read from the onset temperature of the probe displacement on the TMA curve. The T_s values of the polyamides are in the range of 273–295 °C (see Table 2). As can be seen, in all cases, the T_s values of the polyamides obtained by TMA are comparable to the T_g values obtained by the DSC experiments. The thermal stability of polyamides was evaluated by TGA in both air and nitrogen atmospheres. Typical TGA curves for polyamide **6f** are shown in Fig. 2. The decomposition temperatures (T_d) at 5% and 10% weight losses in nitrogen and air atmosphere taken from the original TGA thermogram are list in Table 2. All of the polymers exhibited good thermal stability; the T_ds of polyamides **6a–6h** at a 10% weight loss were in the range of 437–535 °C in nitrogen and 433–512 °C in air, respectively. The amount of carbonized residue (char yield) at 800 °C in nitrogen for the aromatic polyamides was in the range of 63 to 73 wt%. The high char yields of these polyamides can be attributed to their high aromatic content.

3.3.3. Electrochemical properties

The electrochemical properties of the polyamides were investigated by cyclic voltammetry (CV) conducted for the cast film on an ITO-coated

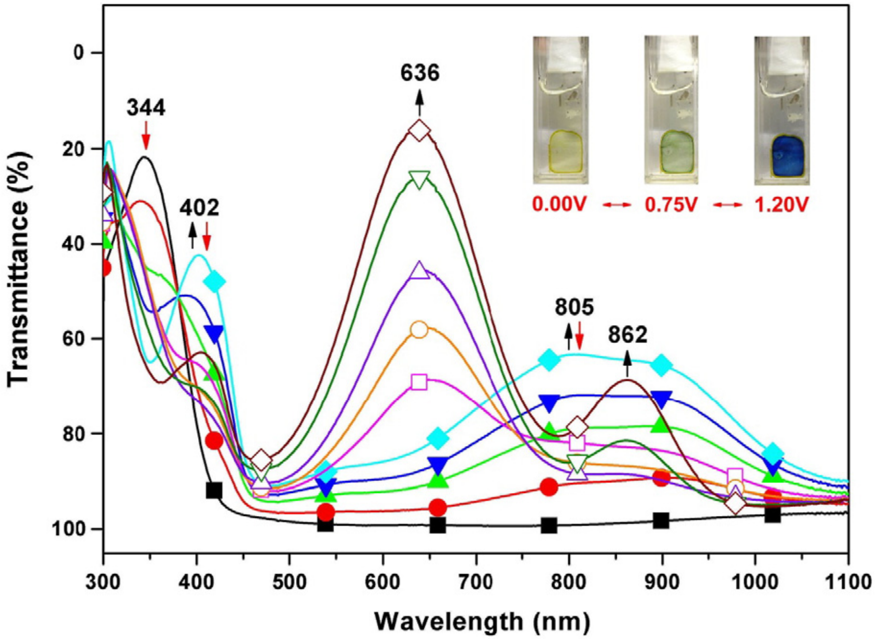

Fig. 4. Spectral change of **6d** thin film on the ITO-coated glass substrate (in MeCN with 0.1 M TBAP as the supporting electrolyte) along with increasing of the applied voltage: 0 (■), 0.50 (●), 0.60 (▲), 0.65 (▼), 0.75 (◆), 0.95 (□), 1.00 (○), 1.05 (△), 1.15 (▽), and 1.20 (◇) vs. Ag/AgCl couple as reference. The inset shows the photographic images of the film at indicated applied voltages. (For interpretation of the references to color in this figure legend, the reader is referred to the web version of this article.)

Please cite this article as: S.-H. Hsiao, et al., Triphenylamine-based redox-active aramids with 1-piperidinyl substituent as an auxiliary donor: Enhanced electrochemical stability..., Reactive and Functional Polymers (2016), http://dx.doi.org/10.1016/j.reactfunctpolym.2016.03.020

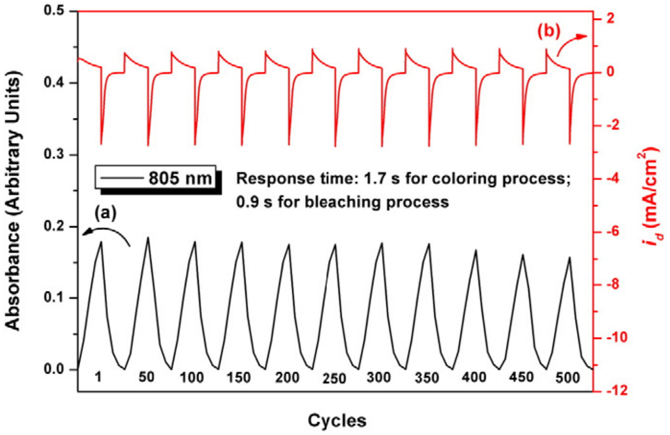

Fig. 6. (a) Potential step absorptiometry and (b) current consumption of the polyamide **6d** film on to the ITO-coated glass substrate (coated area ~1 cm^2) during the continuous cycling test by switching potentials between 0 and 0.75 V (vs. Ag/AgCl) with a cycle time of 4 s.

glass slide as working electrode in anhydrous acetonitrile (MeCN), using 0.1 M of TBAP as supporting electrolyte. Typical CV diagrams for polyamides **6d** and **6d′** are illustrated in Fig. 3. There are two reversible oxidation redox couples at $E_{1/2} = 0.46$ and 0.84 V, respectively, for polyamide **6d** and one reversible oxidation redox couple at $E_{1/2} = 0.86$ V for polyamide **6d′** in the oxidative scan. Polyamide **6d** revealed a relatively lower onset oxidation potential ($E_{\text{onset}} = 0.30$ V) in comparison with its parent analog **6d′** ($E_{\text{onset}} = 0.72$ V). This indicates that the first oxidation wave in the CV diagram of polyamide **6d** is associated with its piperidinyl groups. It was also found that the **6d** film changed color from the pale yellowish neutral state to green and then to deep blue oxidation states. The oxidative and electrochromic reversibility of the polyamide **6d** is maintained on repeated scanning between 0 and 1.2 V (vs. Ag/AgCl). This result confirms that para-substitution of the piperidinyl group on the TPA unit lends considerable stability to both the cation radical and dication quinonediimine species, as shown in Scheme 3. The other polyamides showed similar CV diagrams to that of **6d**. The redox potentials of the polyamides as well as their respective HOMO and LUMO energy levels (vs. vacuum) are shown in Table 3. The external ferrocene/ferrocenium (Fc/Fc$^+$) redox standard $E_{1/2}$ (Fc/Fc$^+$) and E_{onset} (Fc/Fc$^+$) was 0.44 V and 0.37 V vs. Ag/AgCl in MeCN. Under the assumption that the HOMO energy level for the ferrocene standard was 4.80 eV with respect to the zero vacuum level, the HOMO energy for polyamides **6a**–**6h** were evaluated to be 4.80–4.85 eV and 4.70–4.78 eV calculated from $E_{1/2}$ and E_{onset}, respectively. The lower ionization potential could suggest an easier hole injection into films from ITO electrodes in electronic device applications.

Table 4
Coloration efficiency of polyamide **6d**.

Cycles[a]	ΔOD_{805}[b]	Q (mC/cm^2)[c]	η (cm^2/C)[d]	Decay (%)[e]
1	0.179	0.712	251	0
50	0.185	0.750	247	1.6
100	0.179	0.724	247	1.6
150	0.178	0.726	245	2.3
200	0.175	0.718	244	2.8
250	0.175	0.722	242	3.6
300	0.177	0.731	242	3.6
350	0.176	0.739	238	5.2
400	0.167	0.703	238	5.2
450	0.161	0.679	237	5.6
500	0.157	0.670	234	6.8

[a] Switch cycles between potential steps: 0.00 ↔ 0.75 V (vs. Ag/AgCl).
[b] Optical density change at 805 nm.
[c] Ejected charge, determined from the in situ experiments.
[d] Coloration efficiency is derived from the equation: $\eta = \Delta OD_{805}/Q$.
[e] Decay of coloration efficiency after cyclic scans.

3.3.4. Electro-optical and electrochromic properties

Following the electrochemical tests, the optical properties of the electrochromic films were evaluated by using spectroelectrochemistry. For these investigations, the polyamide film was cast on an ITO-coated glass slide (a piece that fit in the commercial UV–visible cuvette), and a homemade electrochemical cell was built from a commercial UV–visible cuvette. The cell was placed in the optical path of the sample light beam in a commercial diode array spectrophotometer. This procedure allowed us to obtain electronic absorption spectra under potential control in a 0.1 M TBAP/MeCN solution. The result of the polyamide **6d** film is presented in Fig. 4 as a series of UV–vis absorbance curves correlated to electrode potentials. In the neutral form, at 0 V, the film exhibited strong absorption at wavelength around 344 nm, characteristic for TPA, but it was almost transparent in the visible region. Upon oxidation of the polyamide **6d** film (increasing applied voltage from 0 to 0.75 V), the intensity of the absorption peak at 344 nm gradually decreased while a new peak at 402 nm and a broad band having its maximum absorption wavelength at 805 nm gradually increased in intensity. We attribute this spectral change to the formation of a stable monocation radical of the (1-piperidinyl)TPA moiety. The absorption band in the near infrared (NIR) region can be attributed to an intervalence charge-transfer (IV-CT) between states in which the positive charge is centered at different amino centers (piperidinyl and TPA units) [57,58]. As the applied potential became more anodic to 1.20 V, the absorption bands of the cation radical decreased gradually in intensity, with the formation of a new strong absorption band centered at around 636 nm and 862 nm. This spectral change can be attributable to the formation of a dication in the (1-piperidinyl)TPA segment of the polyamide. The observed UV–vis absorption changes in the film of **6d** at various potentials are fully reversible and are associated with strong color changes; indeed, they even can be seen readily by the naked eye. From the inset shown in Fig. 4, it can be seen that the film of **6d** switches from a transmissive neutral state (pale yellow) to a highly absorbing semi-oxidized state (green) and a fully oxidized state (deep blue). The film colorations are distributed homogeneously across the polymer film and survive for more than hundreds of redox cycles. The polyamide **6d** shows good contrast in the visible region, with a very high optical transmittance change (Δ%T) of 83% at $\lambda_{\max} = 636$ nm.

For optical switching studies, polymer films were cast on ITO-coated glass slides in the same manner as described above, and each film was potential stepped between its neutral (0 V) and first oxidized (+0.50 V) state. While the films were switched, the absorbance at 805 nm was monitored as a function of time with UV–vis-NIR spectroscopy. Switching data for the cast film of polyamide **6d** are given in Fig. 5. The switching time was calculated at 90% of the full switch because it is difficult to perceive any further color change with naked eye beyond this point. The polyamides switch rapidly (within two seconds) between the highly transmissive neutral state and the colored oxidized state. Thin film of polyamide **6d** required only 1.7 s at 0.75 V for coloring and 0.9 s for bleaching, reflecting the different reaction rates between the neutral and oxidized forms of the film of **6d**. As shown in Fig. 6, the absorbance changes at 805 nm reflect the switch in current, and the kinetics of the charge transport process can be referenced to the coloration response time. The electrochromic coloration efficiencies ($\eta = \Delta OD_{805}/Q$) after various switching steps of the film of polyamide **6d** are summarized in Table 4. The electrochromic film of **6d** was found to exhibit high coloration efficiencies up to 251 cm^2/C at 805 nm, and to retain near 93% of its optical response after 500 coloring/bleaching cycles. Therefore, the electrochromic switching behavior appears to be a highly reversible process.

4. Conclusions

A new TPA-based aromatic diamine monomer, 4,4′-diamino-4″-(1-piperidinyl)triphenylamine, was successfully synthesized in high purity and good yield. Novel (1-piperidinyl)TPA-functionalized aromatic polyamides have been readily prepared from the newly synthesized diamine monomer with various aromatic dicarboxylic acids via the phosphorylation polyamidation reaction. All the polymers were amorphous with good solubility in many polar aprotic solvents and could be solution-cast into flexible and tough films with high thermal stability. Incorporating the piperidinyl substituent on the TPA unit greatly lowered the oxidation potentials of the polyamides. These polymers also revealed multi-color electrochromic behavior, high coloration efficiency, good electrochromic reversibility and rapid switching times. Thus, these characteristics suggest that these new aramids have great potential for use in optoelectronics applications.

Acknowledgements

We thank the Ministry of Science and Technology (MOST 104-2221-E-027-106) of Taiwan for the financial support.

Appendix A. Supplementary data

Supplementary data to this article can be found online at http://dx.doi.org/10.1016/j.reactfunctpolym.2016.03.020.

References

[1] P.M.S. Monk, R.J. Mortimer, D.R. Rosseinsky, Electrochromism: Fundamentals and Applications, VCH, Weinheim, Germany, 1995.
[2] P.M.S. Monk, R.J. Mortimer, D.R. Rosseinsky, Electrochromism and Electrochromic Devices, Cambridge University Press, Cambridge, UK, 2007.
[3] R. Baetens, B.P. Jelle, A. Gustavsen, Sol. Energy Mater. Sol. Cells 94 (2010) 87–105.
[4] C.G. Granqvist, Thin Solid Films 564 (2014) 1–38.
[5] C. Ma, M. Taya, C.Y. Xu, Polym. Eng. Sci. 48 (2008) 2224–2228.
[6] A.M. Osterholm, D.E. Shen, J.A. Kerszulis, R.H. Bulloch, M. Kuepfert, A.L. Dyer, J.R. Reynolds, ACS Appl. Mater. Interfaces 7 (2015) 1413–1421.
[7] R.J. Mortimer, A.L. Dyer, J.R. Reynolds, Displays 27 (2006) 2–18.
[8] P.M. Beaujuge, S. Ellinger, J.R. Reynolds, Nat. Mater. 7 (2008) 795–799.
[9] S. Beaupre, A.-C. Breton, J. Dumas, M. Leclerc, Chem. Mater. 21 (2009) 1504–1513.
[10] www.gentex.com (accessed: December 2015).
[11] G.A. Niklasson, C.G. Granqvist, J. Mater. Chem. 17 (2007) 127–156.
[12] D.T. Gillapie, R.C. Tenent, A.C. Dillon, J. Mater. Chem. 20 (2010) 9585–9592.
[13] L.B. Groenendaal, G. Zotti, P.-H. Aubert, S.M. Waybright, J.R. Reynolds, Adv. Mater. 15 (2003) 855–879.
[14] R.M. Walczak, J.R. Reynolds, Adv. Mater. 18 (2006) 1121–1131.
[15] A. Patra, M. Bendikov, J. Mater. Chem. 20 (2010) 422–433.
[16] G. Gunbas, L. Toppare, Chem. Commun. 48 (2012) 1083–1101.
[17] F.S. Han, M. Higuchi, D.G. Kurth, Adv. Mater. 19 (2007) 3928–3931.
[18] A. Maier, A.R. Rabindranath, B. Tieke, Adv. Mater. 21 (2009) 959–963.
[19] M. Schott, H. Lorrmann, W. Szczerba, M. Beck, D.G. Kurth, Sol. Energy Mater. Sol. Cells 126 (2014) 68–73.
[20] C.W. Hu, T. Sato, J. Zhang, S. Moriyama, M. Higuchi, ACS Appl. Mater. Interfaces 6 (2014) 9118–9125.
[21] P.M. Beaujuge, J.R. Reynolds, Chem. Rev. 110 (2010) 268–320.
[22] P.M. Beaujuge, C.M. Amb, J.R. Reynolds, Acc. Chem. Res. 43 (2010) 1396–1407.
[23] C.M. Amb, A.L. Dyer, J.R. Reynolds, Chem. Mater. 23 (2011) 397–415.
[24] A.L. Dyer, E.J. Thompson, J.R. Reynolds, ACS Appl. Mater. Interfaces 3 (2011) 1787–1795.
[25] J.A. Kerszulis, K.E. Johnson, M. Kuepfert, D. Khoshabo, A.L. Dyer, J.R. Reynolds, J. Mater. Chem. C 3 (2015) 3211–3218.
[26] H.H. Yang, Aromatic High-Strength Fibers, John Wiley & Sons, New York, 1989.
[27] J.M. Garcia, F.C. Garcia, F. Serna, J.L. de la Pena, Prog. Polym. Sci. 35 (2010) 623–686.
[28] S.H. Hsiao, C.F. Chang, Macromol. Chem. Phys. 197 (1996) 1255–1272.
[29] S.H. Hsiao, C.H. Yu, J. Polym. Res. 3 (1996) 247–256.
[30] S.H. Hsiao, C.Y. Yang, Macromol. Chem. Phys. 198 (1997) 2111–2119.
[31] S.H. Hsiao, K.Y. Chu, J. Polym. Sci. A Polym. Chem. 35 (1997) 3385–3391.
[32] C.P. Yang, S.H. Hsiao, H.W. Yang, Polym. J. 31 (1999) 359–363.
[33] S.H. Hsiao, C.P. Yang, M.H. Chuang, S.J. Lin, J. Polym. Sci. A Polym. Chem. 37 (1999) 4510–4520.
[34] S.H. Hsiao, C.P. Yang, S.H. Chen, Polymer 41 (2000) 6537–6551.
[35] G.S. Liou, S.H. Hsiao, J. Polym. Sci. A Polym. Chem. 40 (2002) 1781–1789.
[36] S.H. Hsiao, Y.H. Chang, Eur. Polym. J. 40 (2004) 1749–1757.
[37] S.H. Hsiao, K.H. Lin, Polymer 45 (2004) 7877–7885.
[38] J.F. Espeso, A.E. Lozano, J. de la Campa, I. Garcia-Yoldi, J. de Abajo, J. Polym. Sci. A Polym. Chem. 48 (2010) 1743–1751.
[39] M. Ghaemy, R. Alizadeh, React. Funct. Polym. 71 (2011) 425–432.
[40] M.D. Damaceanu, R.D. Rusa, A. Nicolescu, M. Bruma, A.L. Rusanov, Polym. Int. 60 (2011) 1248–1258.
[41] P. Bandyopadhyay, D. Bera, S. Ghosh, S. Banerjee, RSC Adv. 4 (2014) 28078–28092.
[42] S. Bisoi, P. Bandyopadhyay, D. Bera, S. Ghosh, S. Banerjee, Eur. Polym. J. 66 (2015) 419–428.
[43] Y. Oishi, H. Takado, M. Yoneyama, M. Kakimoto, Y. Imai, J. Polym. Sci. A Polym. Chem. 28 (1990) 1763–1769.
[44] G.S. Liou, S.H. Hsiao, M. Ishida, M. Kakimoto, Y. Imai, J. Polym. Sci. A Polym. Chem. 40 (2002) 2810–2818.
[45] G.S. Liou, S.H. Hsiao, J. Polym. Sci. A Polym. Chem. 41 (2003) 94–105.
[46] M. Thelakkat, Macromol. Mater. Eng. 287 (2002) 442–461.
[47] Y. Shirota, H. Kageyama, Chem. Rev. 107 (2007) 953–1010.
[48] E.T. Seo, R.F. Nelson, J.M. Fritsch, L.S. Marcoux, D.W. Leedy, R.N. Adams, J. Am. Chem. Soc. 88 (1966) 3498–3503.
[49] R.F. Nelson, R.N. Adams, J. Am. Chem. Soc. 90 (1968) 3925–3930.
[50] S.C. Creason, J. Wheeler, R.F. Nelson, J. Organomet. Chem. 37 (1972) 4440–4446.
[51] S.H. Cheng, S.H. Hsiao, T.H. Su, G.S. Liou, Macromolecules 38 (2005) 307–316.
[52] H.J. Yen, G.S. Liou, Polym. Chem. 3 (2012) 255–264.
[53] C.W. Chang, G.S. Liou, S.H. Hsiao, J. Mater. Chem. 17 (2007) 1007–1015.
[54] S.H. Hsiao, G.S. Liou, Y.C. Kung, H.J. Yen, Macromolecules 41 (2008) 2800–2808.
[55] S.H. Hsiao, Y.H. Hsiao, Y.R. Kung, J. Polym. Sci. A Polym. Chem. 54 (2016) 1289–1298.
[56] N. Yamazaki, M. Matsumoto, F. Higashi, J. Polym. Sci. Polym. Chem. Ed. 13 (1975) 1373–1380.
[57] M.B. Robin, P. Day, Inorg. Chem. Radiochem. 10 (1968) 247–422.
[58] C. Lambert, G. Noll, J. Am. Chem. Soc. 121 (1999) 8434–8442.

Please cite this article as: S.-H. Hsiao, et al., Triphenylamine-based redox-active aramids with 1-piperidinyl substituent as an auxiliary donor: Enhanced electrochemical stability..., Reactive and Functional Polymers (2016), http://dx.doi.org/10.1016/j.reactfunctpolym.2016.03.020